Plasmonics
DOI 10.1007/s11468-015-0035-y

Side-Coupled Cavity-Induced Fano Resonance and Its Application in Nanosensor

Zhao Chen [1,2] · Xueyan Cao [1,2] · Xiaokang Song [1,2] · Lulu Wang [1,2] · Li Yu [1,2]

Received: 18 April 2015 / Accepted: 26 July 2015

Abstract A compact structure based on plasmonic metal-insulator-metal (MIM) side-coupled cavities for nanosensor is proposed and numerically simulated. Simulation results show that a typical Lorentzian and Fano-like response emerge in the transmission spectrum, and they can be easily tuned by changing the length of the side cavity and the material imbedded in the resonator. Based on above analysis, our structures offer flexibility to design nanosensor with a sensitivity of ~1820 nm/RIU and a figure of merit about 4.5×10^4. By adding another side-coupled cavity, multiple Fano resonances are achieved and the sensing properties are also investigated. Our structures may have important potential applications in highly integrated optical circuits and networks, especially for nanosensor, spectral splitter, and nonlinear devices.

Keywords Surface plasmons · Fano resonance · Sensor · Integrated optics devices

Introduction

Surface plasmon polaritons (SPPs) are considered to be the most promising candidate for the realization of highly integrated optical circuits, due to their capability to overcome the diffraction limit of light [1]. In particular, the metal-insulator-metal (MIM) waveguides based on SPPs has deep subwavelength field confinements and low bend loss, and thus, it has important applications in highly integrated photonic circuits [2–4]. Compact and light-weight diagnostic devices hold significant promise for early detection and monitoring of diseases in field settings. Plasmonic nanosensors are one of the key components [5–7]. Compared with other types of sensors, the plasmonic waveguide integrated sensor has an inherent advantage to achieve high integration [8, 9]. Recently, Liu et al. designed a planar plasmonic sensing device based on electromagnetically induced transparency [10]. Lu et al. proposed a nanosesor based on Fano interference in a dual cavities system [11], and so on. Among all the nanostructures, the MIM waveguide structures have attracted many researchers' attention due to their deep-sub-wavelength confinement of light [12–15]. These structures are more suitable for the highly integrated optical circuits.

In this paper, a simple and compact plasmonic sensor based on MIM waveguide-coupled structure is proposed. The transmission properties of the structure is investigated by the finite element method. Simulation results show that the resonant peaks can be easily tuned by changing the length of the side-coupled cavity and the material embedded in the resonator. Moreover, other two plasmonic sensor structures are designed by extending the structure to double side-coupled cavities systems. The proposed structures can serve as excellent plasmonic sensor devices with a sensitivity of ~1820 nm/RIU and a figure of merit about $\sim4.5\times10^4$. The proposed structure can find wide applications in the plasmonic nanosensing area.

Structure and Simulations

The illustration in Fig. 1a shows that the investigated waveguide system is simply composed of a MIM

✉ Li Yu
bupt.yuli@gmail.com

[1] State Key Laboratory of Information Photonics and Optical Communications, Beijing University of Posts and Telecommunications, Beijing 100876, China

[2] School of Science, Beijing University of Posts and Telecommunications, Beijing 100876, China

Published online: 14 August 2015

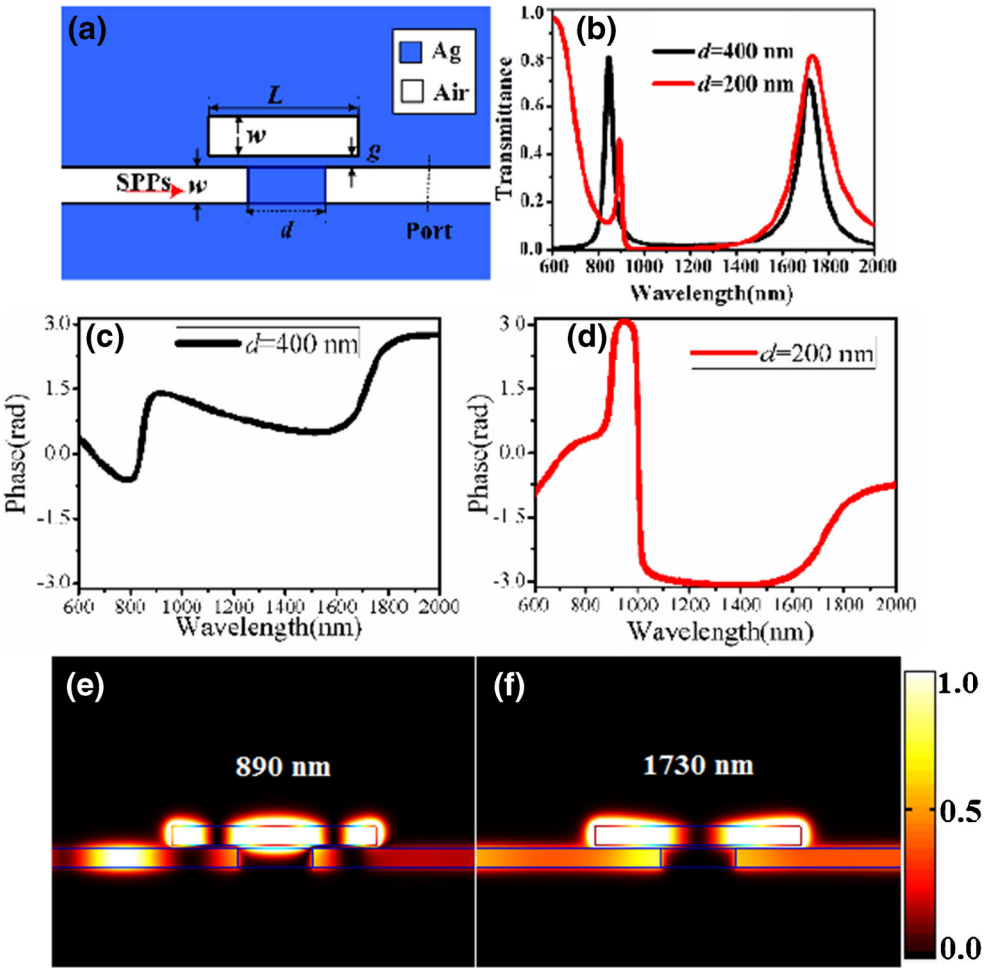

Fig. 1 **a** Schematic configuration and geometric parameters of the plasmonic waveguide system. **b** Transmission spectra with d=400 nm (*black curve*) and d=200 nm (*red curve*) of the system. The parameters are set as L=550 nm. **c, d** Corresponding phase response. **e**, **f** The $|H_z|^2$ field distributions at the resonance wavelength λ=890 nm and λ=1730 nm at d=200 nm

waveguide and a side-coupled cavity. This MIM waveguide structure is very simple, and the ion beam etching (IBE) method can be used to process the insulating air layer waveguide; particle sputtering method can be used

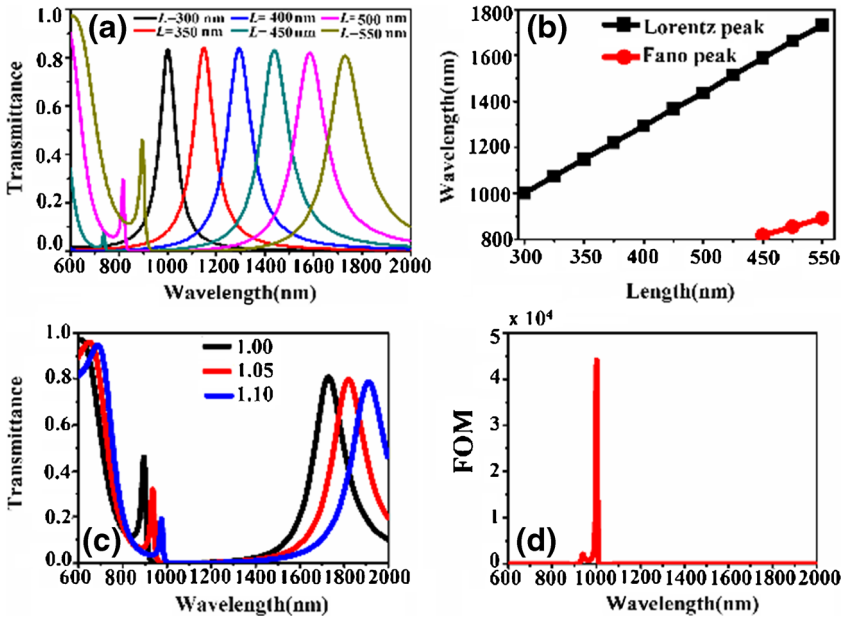

Fig. 2 **a** Transmission spectra of the optical system for different lengths of the side-coupled cavity. **b** Dependence of the resonant wavelengths on length L. **c** Transmission spectra of the optical system for different refractive index in the side-coupled cavity. **d** Calculated FOM at different wavelengths

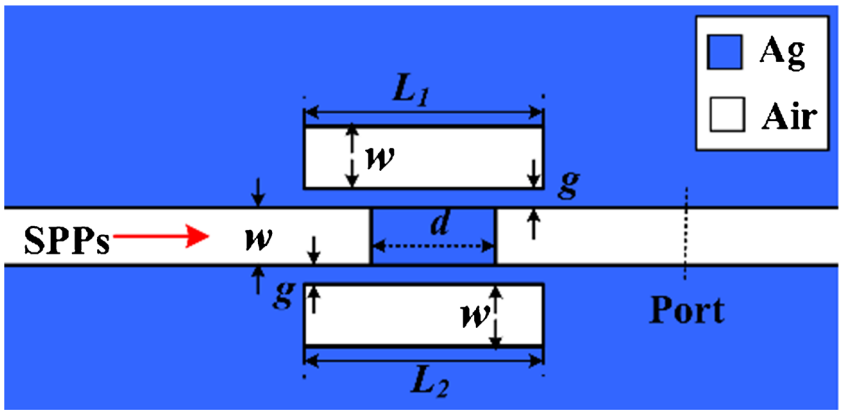

Fig. 3 Schematic of the optical system consisting of a MIM waveguide with two side-coupled cavities in each side, a metal barrier, and the geometrical parameter symbols

to fill the dielectric core. A coupling grating can be served as a SPP generator, and a decoupling grating can be served as a collector. A nano-spectroscopy measurement system can be used to measure the transmission properties. Herein, w denotes the width of the waveguide and cavity and L is the length of the cavity. g stands for the coupling distance between the waveguide and the cavity. In contrast to the ordinary side-coupled system [16], a metal barrier, with thickness d, is introduced in the bus waveguide. The value of d is much bigger than skin depth of SPPs in metal, so that SPPs cannot directly transmit through the barrier to the output port. This system is a two-dimensional model, and the materials in the blue and white areas are chosen to be silver (ε_m), which is characterized by the Drude model [17, 18], and air (ε_d= 1.0), respectively. The transmittance of SPPs is defined as the quotient between the SPP power flows of the observing port with structures (barrier and side-coupled cavity) and without structures [17, 19]. The power flows at the port were obtained by integrating the Poynting vector over the channel cross-section. In the simulations, the parameters are set as follows: L=550 nm, w=50 nm, g= 10 nm, and the values of w and g are fixed throughout this paper.

The transmission properties of the waveguide system are numerically investigated using the finite element method (FEM) with COMSOL Multiphysics. The calculated transmission spectra are displayed in Fig. 1b, red curve for d=200 nm and black curve for d=400 nm, respectively. Figure 1c, d shows the corresponding phase response. It is obviously observed that two symmetric Lorentzian profiles emerge in the transmission spectrum (black curve in Fig. 1b) when d=400 nm. However, the change of d makes the amplitude phase change significantly (see Fig. 1c, d) at the high energy position (600~ 1300 nm), which results in a great difference in the transmission spectrum (red line in Fig. 1b). While at the low energy position (1300~2000 nm), the amplitude phase almost unchanged, brings about few changes in the transmission spectrum. This sharp and asymmetric profile, usually termed as Fano profile [20, 21], results from the higher-order mode excited [22]. The field distributions of $|H_z|^2$ for d=200 nm at λ=890 nm and at λ=1730 nm are shown in Fig. 1e, f, respectively. It is found that the resonant energy is mainly confined in the side-coupled cavity, and higher-order mode is excited at λ=890 nm (Fig. 1e).

Next, we investigated the transmission properties of the proposed structure using FEM. Figure 2a shows the calculated transmission spectra for different length of the side-coupled cavity. Figure 2b displays the dependence of the resonant wavelengths on length L. Herein, d is fixed to 200 nm. It is obvious that both the Fano and Lorentzian peaks are proportional to the length L. According to the simulation results, the

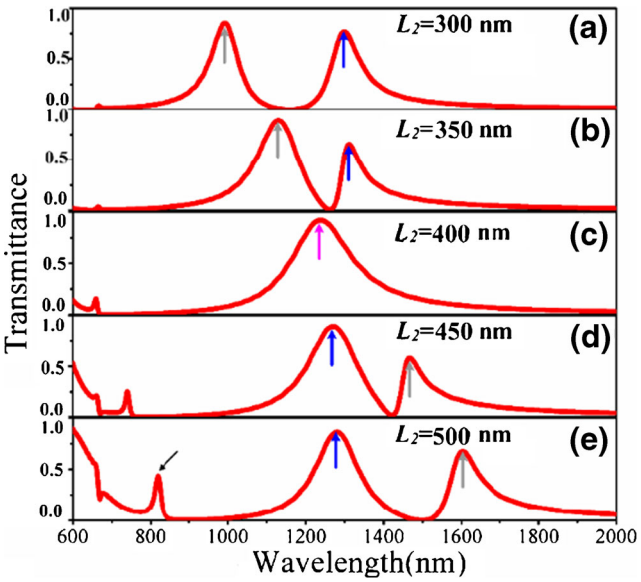

Fig. 4 Simulation results of the transmission spectra at L_1=400 nm; **a** L_2=300 nm, **b** L_2=350 nm, **c** L_2=400 nm, **d** L_2=450 nm, and **e** L_2= 500 nm

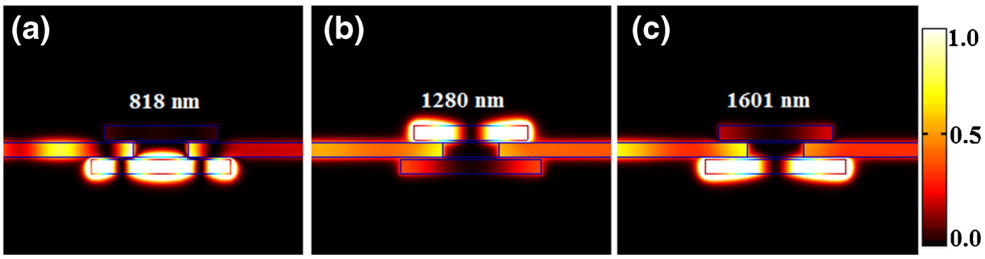

Fig. 5 Corresponding field distributions ($|H_z|^2$) of the Fig. 3e at L_1=400 nm and L_2=500 nm for **a** λ=818 nm, **b** λ=1280 nm, and **c** λ=1601 nm

resonant wavelengths can be easily manipulated by adjusting the length of the side-coupled cavity.

Successively, we investigate the influence of the material embedded in the side-coupled cavity on the resonant wavelengths. The length of the side-coupled cavity is set to be 550 nm. By changing the refractive index, the center wavelength exhibits a red shift as shown in Fig. 2c. It is found that the resonance wavelength varies linearly with the refractive index. Besides, for some liquid substance [water (n=1.33) or ethanol (n=1.36)], even solid matter [silica (n=1.5)], the proposed structure and the linear rule are still applicative, for example, L=400 nm and d=200 nm. Therefore, one can simply manipulate the resonant wavelengths by fitting the material with appropriate refractive index in the side-coupled cavity. This feature provides an excellent scheme for the applications toward nanoscale sensing. The sensitivity of a sensor (nm/RIU) is usually defined as the shift in the resonance wavelength per unit variations of the refractive index [23]. Thus, the sensitivity of the proposed structure is 900 nm/RIU for Fano resonance and 1820 nm/RIU for Lorentzian resonance. These results are higher than those in the references [10, 23]. To better evaluate the performance of the plasmonic sensor, the figure of merit (FOM) is studied, which is defined as FOM=$\Delta T/(T\Delta n)$ [24], where T denotes the transmittance in the proposed structure. The calculated FOM are displayed in Fig. 2d. The values of FOM is as high as ~4.5×10^4 at λ=1000 nm, which is due to the sharp asymmetric Fano line shape with ultra-low transmittance at this wavelength.

Multiple Side-Coupled Cavities Systems

The proposed structure in Fig. 1a is flexible and can be easily extended to a multiple side cavities system by adding another side-coupled cavity, as shown in Fig. 3. In this case, the two cavities cannot interact with each other, so one portion of SPPs

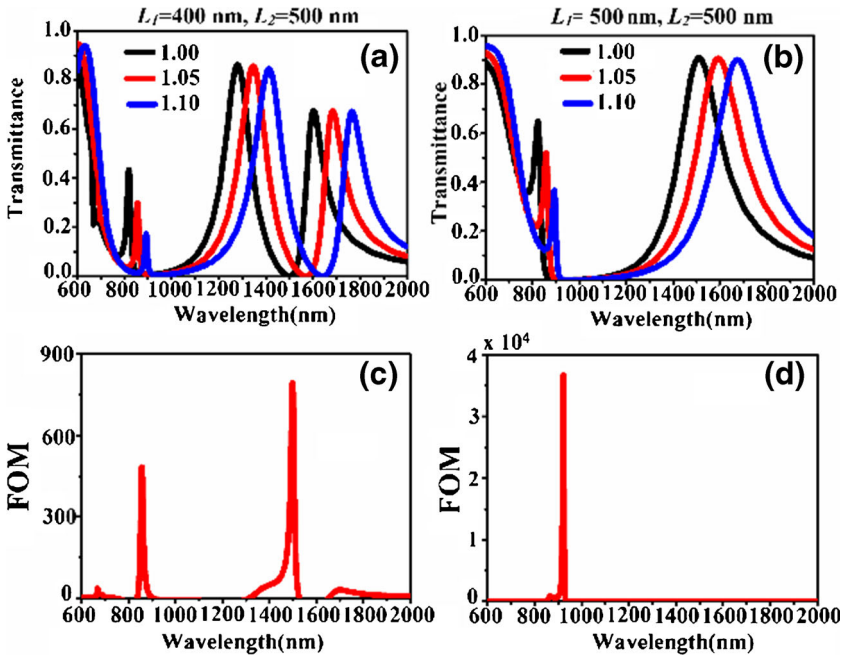

Fig. 6 Transmission spectra of the optical system for different refractive index in the side-coupled cavity **a** L_1=400 nm and L_2=500 nm, and **b** L_1=500 nm and L_2=500 nm. **c**, **d** The corresponding calculated FOM at different wavelengths

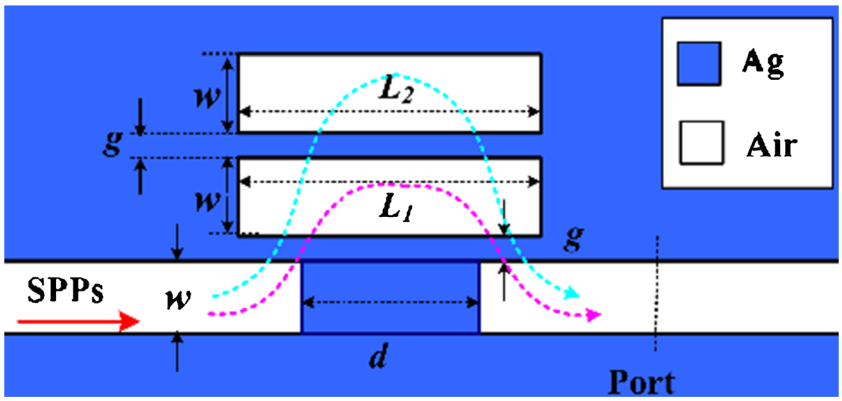

Fig. 7 Schematic of the optical system consisting of a MIM waveguide with two side-coupled cavities in one side, a metal barrier, and the geometrical parameter symbols

coupled to the upper cavity and the other to the lower cavity will propagate to the output port. By carefully adjusting the parameters of the structure, we can separate the two different paths of SPPs. To display the phenomenon intuitively, the transmission spectra of the proposed structure are simulated with FEM and the calculated transmission spectra are shown in Fig. 4a–e. It is obviously observed that two resonant peaks emerge in the transmission spectra. Moreover, one of them exhibits a red shift [denoted by the gray arrows] with L_2 increases, the other keeps almost unchanged [denoted by blue arrows] due to L_1 is fixed to 400 nm. That is to say, the gray-arrow denoted Fano peaks are determined by the lower cavity, while the others are determined by the upper cavity. Figure 5a–c shows the corresponding field distributions of $|H_z|^2$ at L_1= 400 nm and L_2=500 nm (Fig. 4e). It is observed that the energy of the resonant peaks is confined in only one side cavity. These behaviors of the two resonances accord well with the analysis.

The sensing properties of the proposed structure are studied in two situations: (a) L_1=400 nm, L_2=500 nm; (b) L_1= 500 nm, L_2=500 nm. The calculated transmission spectra with different refractive index and FOM are displayed in Fig. 6. This structure yields a sensitivity about 760, 1320, and 1640 nm/RIU with the max of FOM=815, 760, and 1640 nm/RIU with the max of FOM=3.7×10^4, for the two cases, respectively. It is found that although the sensitivity of the two cases are almost the same, the difference of max value of FOM is very big. This is due to the strong resonance when the two side cavities have the same resonant wavelength, which makes an ultra-low transmittance at this wavelength.

In addition to the above case, the structure proposed in Fig. 1a can also extend to the other situation, shown as in Fig. 7. The propagation behaviors of SPPs can be illustrated by the two dotted lines, and these SPPs with different paths will be interference with each other at the output port, which may enrich the transmission spectra.

To better demonstrate the phenomena, the transmission spectra are calculated, which are shown in Fig. 8a–e. It is found that two resonant peaks appear in the transmission spectra, and both of them are red shift linearly [denoted by the dotted lines]. In order to understand the underlying physics of the resonant peaks in the transmission spectra, the field distributions of H_z at

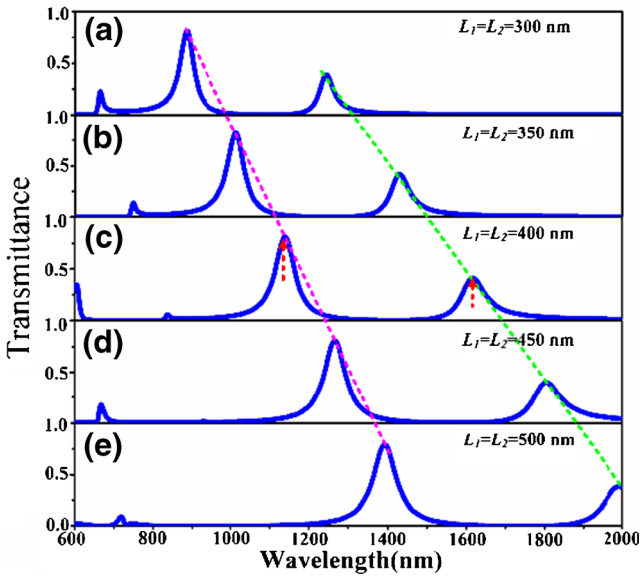

Fig. 8 Simulation results of the transmission spectra at **a** L_1=L_2= 300 nm, **b** L_1=L_2=350 nm, **c** L_1=L_2=400 nm, **d** L_1=L_2=450 nm, and **e** L_1=L_2=500 nm

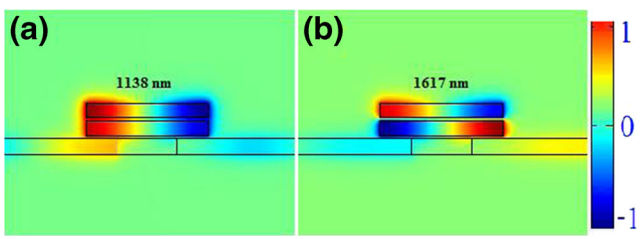

Fig. 9 Corresponding field distributions (Hz) of Fig. 7 at L_1=400 nm and L_2=400 nm for **a** λ=1138 nm and **b** λ=1617 nm

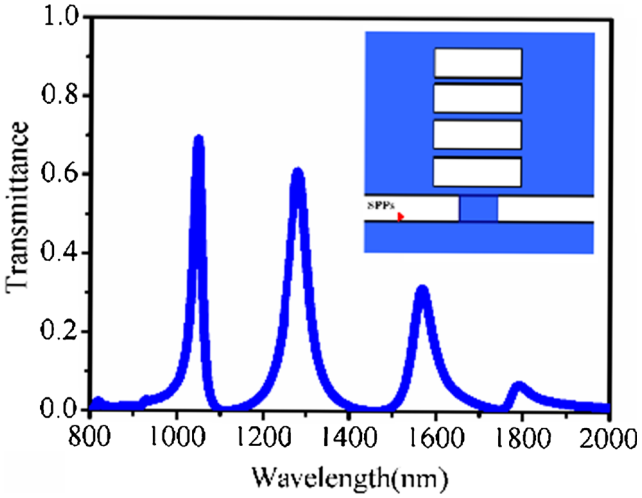

Fig. 10 Transmission spectrum of the four resonator-coupled system. *Inset* shows the schematic of the four resonator-coupled system

the resonant peaks [denoted by the red arrows], with L_1= 400 nm and L_2=400 nm, are displayed in Fig. 9a–b. Obviously, the two resonant peaks [one is high energy, denoted by the pink dotted line, the other is low energy, denoted by the green dotted line] are aroused by the lower resonant mode, and they are degenerate. The difference between the two resonant peaks is that the phase of H_z in the adjacent of the two side-coupled cavities are inphase and antiphase for the high-energy and low-energy Fano peak [25], respectively.

According to the above analysis, the structure of Fig. 7 can be easily extended to a four resonator-coupled system (inset in Fig. 10). Figure 10 shows the transmission spectrum of the system. Herein, the four side-coupled cavity are set, for simplicity, the same with L=400 nm. It is obvious that four Fano resonance peaks occur in the transmission spectrum, which are caused by the complex interference with multiple paths of SPPs. The multi-resonator-coupled system with multi-Fano profiles optical responses may have complex functional applications, such as sensors, splitters multichannel switches, and wavelength-division multiplexing.

Summary

In summary, the sensing characteristics of the proposed structure, which consists of a MIM waveguide with a side-coupled cavity and a metal barrier, are analyzed and investigated. Simulation results show that a typical Lorentzian and Fano-like response emerge in the transmission spectrum, and they can be easily tuned by changing the length of the side cavity and the material imbedded in the resonator. Based on the above analysis, a nanosensor with a sensitivity 1820 nm/RIU and a figure of merit about 4.5×10^4 is achieved. By extending the simple structure to multiple resonator systems, multiple Fano profiles can be achieved. Our structures may have important potential applications in highly integrated optical circuits and networks, especially for nanosensor, spectral splitter, and nonlinear devices.

Acknowledgments This work was supported by the National Natural Science Foundation of China under Grants No.11374041, 11404030 and Fund of State Key Laboratory of Information Photonics and Optical Communications (Beijing University of Posts and Telecommunications), P. R. China.

References

1. Barnes WL, Dereux A, Ebbesen TW (2003) Surface plasmon subwavelength optics. Nature 424(6950):824–830
2. Xu T, Wu YK, Luo XG, Guo LJ (2010) Plasmonic nanoresonators for high-resolution colour filtering and spectral imaging. Nat Commun 1:59
3. Veronis G, Fan SH (2005) Bends and splitters in metal-dielectric-metal subwavelength plasmonic waveguides. Appl Phys Lett 87: 131102
4. Economou EN (1969) Surface plasmons in thin films. Phys Rev 182:539
5. Mayer KM, Hafner JH (2011) Localized surface plasmon resonance sensors. Chem Rev 111:3828–3857
6. Cetin AE, Coskun AF, Galarreta BC, Huang M, Herman D, Ozcan A, Altug H (2014) Handheld high-throughput plasmonic biosensor using computational on-chip imaging. Light Sci Appl 3(122):1–10
7. Coskun AF, Cetin AE, Galarreta BC, Alvarez DA, Altug H, Ozcan A (2014) Lensfree optofluidic plasmonic sensor for real-time and label-free monitoring of molecular binding events over a wide field-of-view. Sci Rep 4(6789):1–7
8. Gramotnev DK, Bozhevolnyi SI (2010) Plasmonics beyond the diffraction limit. Nat Phonotics 4:83–91
9. Ozbay E (2006) Plasmonics: merging photonics and electronics at nanoscale dimensions. Science 311:189
10. Liu N, Weiss T, Mesch M, Langguth L, Eigenthaler U, Hirscher M, Sonnichsen C, Giessen H (2010) Planar metamaterial analogue of electromagnetically induced transparency for plasmonic sensing. Nano Lett 10:1103–1107
11. Lu H, Liu XM, Mao D, Wang GX (2012) Plasmonic nanosensor based on Fano resonance in waveguide-coupled resonators. Opt Lett 37(18):3780–3782
12. Chen Z, Chen JJ, Yu L, Xiao JH (2014) Sharp trapped resonances by exciting the anti-symmetric waveguide mode in a metal insulator metal resonator. Plasmonics 10(1):131–137
13. Lu H, Liu X, Mao D, Gong Y, Wang G (2011) Induced transparency in nanoscale plasmonic resonator systems. Opt Lett 36(16):3233–3235
14. Wen KH, Yan LS, Pan W, Luo B, Guo Z, Guo YH, Luo XG (2014) Electromagnetically iInduced transparency-like transmission in a compact side-coupled T-shaped resonator. J Lightwave Technol 32(9):1071–1707
15. Chen JJ, Wang C, Zhang R, Xiao JH (2013) Multiple plasmon-induced transparencies in coupled-resonator systems. Opt Lett 37(24):5133–5135
16. Zhang Q, Huang XG, Lin XS, Tao J, Jin XP (2009) A subwavelength coupler-type MIM optical filter. Opt Express 17(9):7549–7554

17. Chen Z, Yu L (2014) Multiple Fano resonances based on different waveguide modes in a symmetry breaking plasmonic system. IEEE Photonics J 6(6):4802208
18. Wang GX, Lu H, Liu XM, Mao D, Duan LN (2011) Tunable multi-channel wavelength demultiplexer based on MIM plasmonic nano-disk resonators at telecommunication regime. Opt Express 19(4): 3513–3518
19. Chen JJ, Li Z, Zou YJ, Deng ZL, Xiao JH, Gong QH (2013) Coupled-resonator-induced Fano resonances for plasmonic sensing with ultra-high figure of merits. Plasmonics 8:1627–1632
20. Fano U (1961) Effects of configuration interaction on intensities and phase shifts. Phys Rev 124:1866–1878
21. Miroshnichenko A, Flach S, Kivshar Y (2010) Fano resonances in nanoscale structures. Rev Mod Phys 82:2257–2298
22. Habteyes TG, Dhuey S, Cabrini S, Schuck PJ, Leone RL (2011) Theta-shaped plasmonic nanostructures: bringing "dark" multipole plasmon resonances into action via conductive coupling. Nano Lett 11:1819–1825
23. Liu N, Mesch M, Weiss T, Hentschel M, Giessen H (2010) Infrared perfect absorber and its application as plasmonic sensor. Nano Lett 10:2342–2348
24. Becker J, Trugler A, Jakab A, Hohenester U, Sonnichsen C (2010) The optimal aspect ratio of gold nanorods for plasmonic bio-sensing. Plasmonics 5:161–167
25. Chen Z, Wang W, Cui L, Yu L, Duan G, Zhao Y, Xiao J (2014) Spectral splitting based on electromagnetically induced transparency in plasmonic waveguide resonator system. Plasmonics 10:721–727